Microvessel occlusions alter amyloid-beta plaque morphology in a mouse model of Alzheimer's disease

Yuying Zhang, Evan D Bander, Yurim Lee, Celia Muoser,
Chris B Schaffer and Nozomi Nishimura [iD]

Abstract

Vascular dysfunction is correlated to the incidence and severity of Alzheimer's disease. In a mouse model of Alzheimer's disease (APP/PS1) using in vivo, time-lapse, multiphoton microscopy, we found that occlusions of the microvasculature alter amyloid-beta ($A\beta$) plaques. We used several models of vascular injury that varied in severity. Femtosecond laser-induced occlusions in single capillaries generated a transient increase in small, cell-sized, $A\beta$ deposits visualized with methoxy-X04, a label of fibrillar $A\beta$. After occlusions of penetrating arterioles, some plaques changed morphology, while others disappeared, and some new plaques appeared within a week after the lesion. Antibody labeling of $A\beta$ revealed a transient increase in non-fibrillar $A\beta$ one day after the occlusion that coincided with the disappearance of methoxy-X04-labeled plaques. Four days after the lesion, anti-$A\beta$ labeling decreased and only remained in patches unlabeled by methoxy-X04 near microglia. Histology in two additional models, sparse embolic occlusions from intracarotid injections of beads and infarction from photothrombosis, demonstrated increased labeling intensity in plaques after injury. These results suggest that microvascular lesions can alter the deposition and clearance of $A\beta$ and confirm that $A\beta$ plaques are dynamic structures, complicating the interpretation of plaque burden as a marker of Alzheimer's disease progression.

Keywords

Stroke, Alzheimer's, two-photon in vivo microscopy, microcirculation, vascular cognitive impairment, microglia, brain imaging, confocal microscopy

Introduction

Vascular health is emerging as a critical factor in Alzheimer's disease (AD). Recent clinical work correlating postmortem pathology with cognitive performance suggests that cerebrovascular damage, such as small strokes, strongly exacerbates dementia in patients with Alzheimer's pathology.[1] There is evidence that the neurological decline in AD begins before the deposition of amyloid-beta ($A\beta$) in plaques, and vascular abnormalities are present even before neurological decline.[2] Risk factors for small strokes and hemorrhages, such as hypertension, diabetes, and smoking, are also risk factors for AD.[3,4] Cerebrovascular disease is commonly observed along with AD pathology.[5] Vascular dementia and AD often occur in the same patient, leading to a diagnosis of "mixed dementia."[2,6] Taken together, this evidence implicates vascular pathology as an important contributing factor in AD-associated dementia.

$A\beta$, the peptide that drives the pathology of AD, is produced by neurons at relatively steady levels throughout life in the majority of patients[7] and cleared from the brain through multiple pathways including through the vessels.[8–10] Events that increase the concentration of $A\beta$ in the brain, either by increasing production or decreasing clearance, are potential initiators

---

Nancy E. and Peter C. Meinig School of Biomedical Engineering, Cornell University, Ithaca, NY, USA

Corresponding author:
Nozomi Nishimura, Cornell University, 117 Weill Hall, 526 Campus Rd., Ithaca, NY 14853, USA.
Email: nn62@cornell.edu

or exacerbators of AD. Animal experiments that model stroke or blood flow reductions have shown that Aβ deposits increase in the margin of a stroke.[11–15] Hypoxia may also increase Aβ accumulation.[16,17] Ischemic and hemorrhagic lesions also lead to increased inflammation, altered protein synthesis, and generation of reactive oxygen species, all of which have been linked to increased Aβ aggregation.[18] Collectively, these data suggest that vascular lesions accelerate Aβ accumulation by locally increasing production or decreasing clearance of Aβ. However, other experiments suggest the opposite relationship, indicating that there are some situations in which inflammation or injury might decrease Aβ deposition.[19–23]

Previous work in animal models investigating the effect of vascular occlusions on Aβ accumulation have tended to focus on the impact of larger strokes, such as those produced by occlusion of the middle cerebral artery.[11–15] In the aging human population, however, occlusions in smaller vessels, often producing no noticeable acute symptoms, are far more common.[4] The impact of these microvascular occlusions on Aβ accumulation has remained unexamined. We hypothesized that such small vessel occlusions that do not cause large infarcts with clinically apparent symptoms could be important modulators of Aβ deposition in AD. Occlusions in the microvasculature (e.g., arterioles and capillaries) from processes such as embolism, lipohylalinosis, or microthrombus formation could thus contribute to the development of dementia both through their direct effects on neurons and other brain cells as well as through their impact on AD pathology.

Here, we used several models of small strokes in a transgenic mouse model of AD to examine how microvascular occlusions affect the formation of new Aβ deposits as well as how they affect pre-existing Aβ plaques. Occlusions of single capillaries using femtosecond laser ablation result in >50% blood flow decrease in only a few downstream branches and no infarcts,[24] while occlusions of penetrating arterioles by focused illumination with rose bengal result in larger numbers of affected vessels and ∼400-μm cortical infarcts.[25–27] A larger, 1–2 mm infarct results from the direct occlusion of hundreds of capillaries by wide-field rose bengal illumination.[28] We also included a mild embolic stroke from microbeads injections through the carotid artery.[29] We found that microvascular lesions alter nearby Aβ deposition in a variety of ways, driving both the appearance and disappearance of Aβ deposits as well as transient rearrangements. These data suggest a complex relationship between vascular occlusions and Aβ accumulation, which may be the source of conflicting results in the literature on the effects of vascular lesions on Aβ deposition.

Materials and methods

Experimental animals

We used both male and female mice with mutated proteins associated with inherited forms of AD (mutated amyloid precursor protein (Mo/HuAPP695swe) and mutant presenilin 1 (PS1-dE9); Jackson Labs strain: B6.Cg-Tg(APPswe, PSEN1dE9)85Dbo/J). They develop dense amyloid plaques throughout the brain by about six months of age, here referred to as APP/PS1.[30] Wild-type controls were age-matched littermates. Animals were group housed, with a 12-h light cycle. Ages ranged from 8 to 28 months. To image plaques and microglia, we crossed the APP/PS1 mice to mice that have green fluorescent protein (GFP) knocked in for the Cx3cr1 gene (B6.129P(Cg)-Ptprca Cx3cr1tm1Litt/LittJ, breeders from Jackson Labs[31]), to create mice with APP/PS1 genes and one intact Cx3cr1 allele. To identify lesions in tissue sections by visualizing neuron degeneration, we crossed the AD-microglia mice to B6.Cg-Tg(Thy1-YFP)HJrs/J (breeders from Jackson Labs). These mice express yellow fluorescent protein (YFP) in a subset of neurons, GFP in microglia and AD-related genes. All the mice expressing GFP in microglia are referred to here as AD-microglia mice and grouped together because we did not see any effects of YFP expression on plaque or microglia dynamics. AD-microglia mice were used at 11–13 months of age. Number of animals used and corresponding age information for each experiment is summarized in Supplementary Table 1. All animal experiments were conducted according to procedures approved by Cornell University's Institutional Animal Care and Use Committee. Cornell University is accredited by the Association for Assessment and Accreditation of Laboratory Animal Care International, and all experiments conform to these guidelines. ARRIVE (Animal Research: Reporting in vivo Experiments) guidelines were followed for reporting results of animal experiments.

In vivo imaging with multiphoton microscopy

Chronic cranial windows were implanted in adult mice (Supplementary Methods). To fluorescently label the microvasculature, we used Texas-red dextran in saline (40 μL, 2.5%, MW = 70 kDa, Invitrogen). We administered 20 to 40 μL methoxy-X04 (1 mg/mL, preparation details in Supplementary Methods), a Congo red derivative that crosses the blood–brain barrier and labels Aβ fibrils,[32] to mice before each imaging session to label Aβ deposition and cerebral amyloid angiopathy (CAA). During image acquisition, mice were maintained under anesthesia with 1%–2% isoflurane in

oxygen and secured in a custom-built stereotactic frame to reduce breathing artifacts. To prevent dehydration, 100 μL of 5% glucose in saline was administered every hour. The breathing rate was maintained at ∼1 Hz by adjusting the inhaled isoflurane concentration. The mouse was kept at 37°C with a feedback-controlled heating pad throughout imaging. Images were obtained on a custom-built multiphoton microscope[27] running ScanImage software.[33]

Femtosecond laser ablation for subsurface vessel occlusion

To occlude single, subsurface vessels, including precapillary arterioles and capillaries, we used femtosecond laser pulses to drive photodisruption within the targeted vessel while imaging with multiphoton microscopy.[25] In brief, 50-fs, 800-nm, 1-kHz laser pulses from a regenerative Ti:Sapphire amplifier (Legend-USP; Coherent, Santa Clara, CA) were aimed into the target vessel. The amount of irradiation was increased gradually from 1 to 1000 pulses starting at low energies (∼50-nJ incident per pulse) to higher energies (maximum ∼500 nJ). Several places along the target segment were irradiated until the motion of red blood cells stopped as visualized by Texas-red dextran injected into the vasculature. Vessels were checked for recanalization for about 2 h and if found flowing, reclotted with repeated irradiation. All vessels occluded using this method were spontaneously flowing again after one day. Control data were taken from ipsilateral regions at least ∼500 μm from lesions in the same imaging windows.

Photothrombotic occlusions of penetrating arterioles with rose bengal

Penetrating arterioles were occluded using photothrombosis during imaging with multiphoton microscopy. Mice were injected retro-orbitally with 50 μL of rose bengal (10 mg/mL in saline) immediately before irradiation. Green laser light (∼5-mW incident power) was focused through the microscope objective into the center of the imaging plane at a targeted penetrating arteriole.[26] Laser irradiation was delivered in 10- to 60-s bouts alternating with imaging, until the arteriole and some of its branches were occluded. This resulted in a ∼100 to 300 μm-wide region with some occluded capillaries within the vicinity of the target vessel. In APP/PS1 animals, separate animals without lesions were used as controls. In AD-microglia animals, the contralateral hemispheres without lesions were used as control.

Image analysis of in vivo multiphoton microscopy of plaques and microglia

To quantify and characterize plaques and microglia, in vivo image stacks were maximum-intensity-projected. Images were then segmented using a threshold based on the average and standard deviation intensity of a manually chosen background region. Respective analyses were done on segmented images (Supplemental Methods and Supplementary Figure 1).

Intact-skull photothrombotic occlusions of vessels within a 1-mm region with rose bengal

For larger lesions that generate cortical infarctions, we irradiated through the intact skull to occlude nearly all vessels in a ∼1 mm wide cortical region. The skin above the skull was injected with 100 μL of 0.125% bupivacaine, retracted and kept wet with saline. Mice were injected retro-orbitally with 50 μL of rose bengal (10 mg/mL in saline) immediately before irradiation. A collimated beam (∼40 mW) with about 1-mm diameter was aimed on the skull about 2-mm lateral and 3-mm caudal to bregma on one side of the skull for 5 min. After irradiation, the skin was closed and these mice were dosed with buprenorphine (0.010 mg/100g) every 8 h for the first 72 h of survival for pain management while minimizing interference with the inflammation due to the lesion. The contralateral hemisphere without lesions was used as control.

Microbead embolic stroke model

During surgery, mice were anesthetized using 5% isoflurane and maintained at 1.5%–2.0%. Glycopyrrolate (0.5 mg/kg mouse) was injected intramuscularly to facilitate respiration. Body temperature was kept constant at 37°C using a heating blanket. An incision was made in the neck and blunt dissection was performed to expose and isolate the left carotid artery. The common and external carotid arteries were temporarily ligated with taut sutures and a small needle (29 G) was guided into the common carotid artery above the ligation. A 100-μL solution containing ∼2000, 25-μm diameter, blue, polystyrene microspheres (Polysciences, Inc., PA, USA) or sterile saline for the sham experiments was slowly injected. The needle was then withdrawn, the puncture in carotid artery allowed to clot, and the neck incision was sutured shut. Animals were given buprenorphine (0.010 mg/100g), every 8 h for three days after the surgery. Animals survived for 5 or 10 days after lesioning. Two animals died within two days after microbead injections and were not counted in the reported animal numbers.

Immunohistochemistry and imaging tissue

At the end of the survival period, animals were transcardially perfused with phosphate-buffered saline (PBS) followed by 4% paraformaldehyde in PBS. Brains were post-fixed, cryoprotected, and sectioned on a cryostat. Microglia were labeled with anti-IBA-1, a rabbit polyclonal antibody (Wako 019-19741) and Aβ was labeled with using polyclonal antibodies, pan-Aβ (MBL International Corporation AT-5001) and Abcam ab2539. Details are provided in Supplementary Methods.

Statistical analysis

When distributions of the data were non-normal, non-parametric statistical tests were used. When comparing plaque properties between lesioned and unlesioned groups the Wilcoxon–Mann–Whitney rank-sum test was implemented. When comparisons were made in two regions of the same animal's brain, injection and contralateral side, Wilcoxon rank signed test for paired data was used. Alpha was set to 0.05. These tests used Kaleidagraph. Box plots show quartiles and medians in boxes, black dots show means, and whiskers show $1.5 \times$ (75th–25th percentile values). When analyzing individual plaques across different days, a Kruskal–Wallis test, which is a non-parametric one-way analysis of variance (ANOVA) test (Graphpad Prism), and multiple comparison test followed by Dunn's correction was used.

Results

To study the interaction between microvascular occlusions and Aβ deposits in the APP/PS1 transgenic mouse model of AD, we used several models of vascular lesions that occluded small brain vessels ranging in size from single capillaries to small arterioles. The injury models also differed in the number of vessels affected, providing a range of severity. To observe changes in Aβ plaque deposition, we used in vivo multiphoton microscopy to image methoxy-X04-labeled, fibrillar Aβ in plaques[32] over timescales of hours to weeks. We also compared the density and morphology of Aβ deposits near and far from microvascular occlusions using antibody labeling in extracted tissue.

Femtosecond laser occlusions of capillaries and pre-capillary arterioles cause the formation of small, transient Aβ deposits

The mildest of our vascular lesion models is the occlusion of a single capillary or pre-capillary arteriole below the cortical surface. During imaging, clots were induced in subsurface pre-capillary arterioles and capillaries by irradiating the vessel wall with tightly focused femtosecond laser pulses to induce clotting in the vessel and stop blood flow.[25] Over several days, we observed an accumulation of fluorescent deposits around the targeted vessel, which included autofluorescence at both green and red wavelengths, as well as fluorescence from Texas-red and methoxy-X04 (Figure 1(a) to (h)). Because the emission spectra of the autofluorescence overlapped that of methoxy-X04, we found it was necessary to linearly unmix the signals from a blue (425 nm center wavelength) and green (530 nm) image to differentiate the two sources of fluorescence. Images from lesioned areas in mice that did not receive methoxy-X04 injections were used to estimate the spectra of the autofluorescence, while spontaneous plaques in animals with no vascular lesions were used to estimate the spectra of pure methoxy-X04. We used the blue and green images to compute an unmixed methoxy-X04 image (e.g., Figure 1(d) and (h), Supplementary Figure 1).

New methoxy-X04-labeled deposits appeared as soon as one day after an occlusion of a single capillary or pre-capillary arteriole (Figure 1 and Supplementary Figure 4). These deposits tended to be smaller ($\sim$5–15 μm in diameter) than spontaneously formed extracellular plaques, which can reach diameters greater than 100 μm. A couple days after the lesion, the methoxy-X04 deposits increased in number and in area per deposit as compared to control regions without lesions (Figure 1(q) to (t)). By two weeks, the number of deposits had returned to pre-occlusion levels. We did, however, see examples where methoxy-X04 deposits that appeared after the occlusion persisted as long as 60 days after the lesion. Similar analysis on the unmixed autofluorescence channels showed autofluorescent deposits remained unaffected in both number and area (Figure 1(u) to (x)). Lesions did not produce detectable methoxy-X04 deposits in wild-type littermates (Supplementary Figure 2). Similar deposits were found to appear after a vessel occlusion in experiments using a thinned-bone window rather than a craniotomy (Supplementary Figure 3).

Pre-existing Aβ plaques change morphology after capillary and penetration arteriole occlusions

After occlusion of single, targeted capillaries and pre-capillary arterioles, the morphology of some nearby, pre-existing plaque, as visualized by methoxy-X04, changed in the days after the lesion to appear more condensed near the middle of the plaque (Figure 2). These changes started to reverse after about one week with the plaques regaining a more "diffuse"
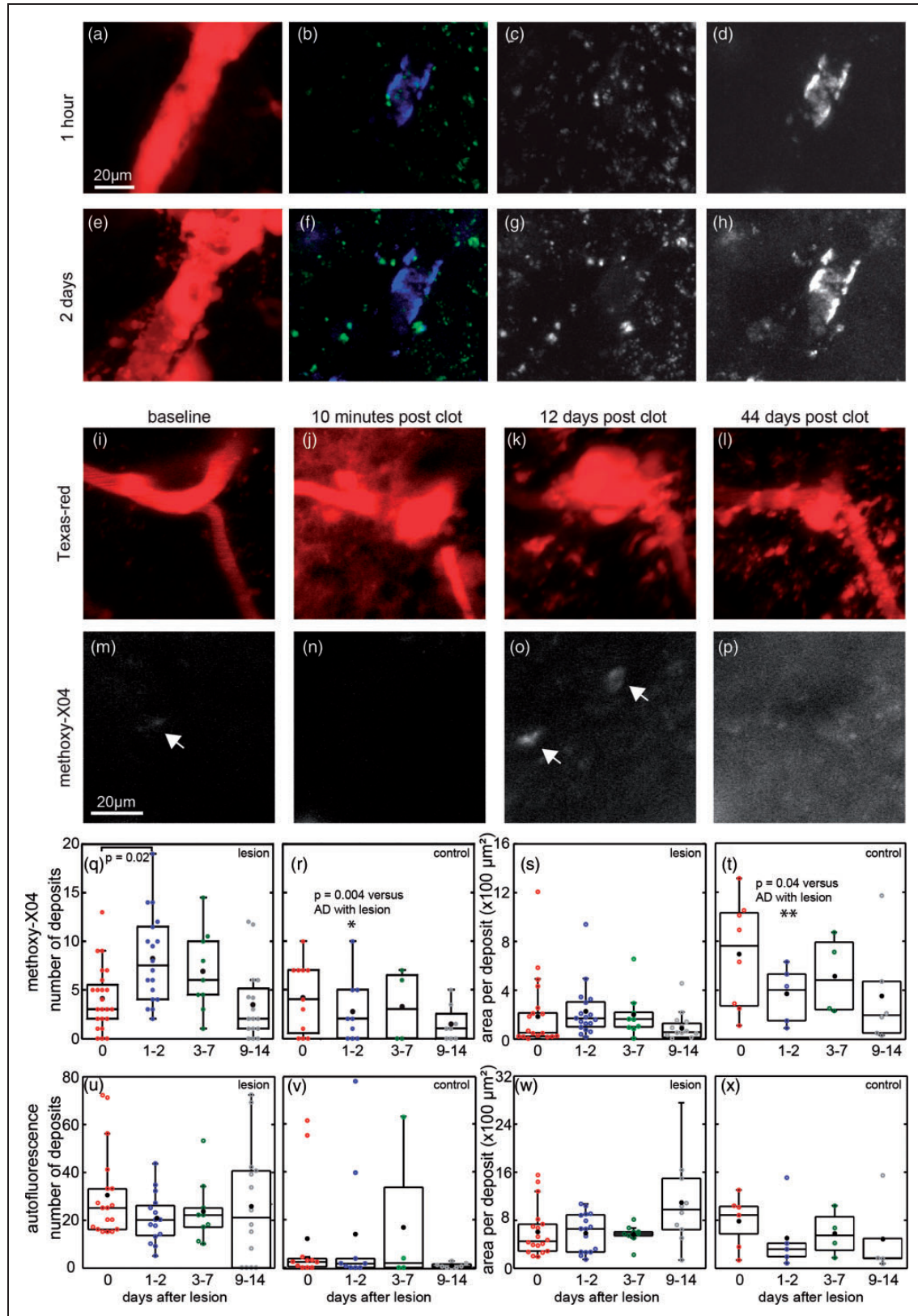
Figure 1. Spectral unmixing of multiphoton microscopy images around laser-induced vascular lesions reveals methoxy-X04 deposits and autofluorescence. Images were taken 1 h (a–d) and two days (e–h) after a pre-capillary arteriole was clotted with femtosecond laser irradiation. Red shows both Texas-red dextran injected into vessels and accumulated autofluorescence (a and e). Spectral

appearance. Pre-existing, parenchymal plaques had much brighter methoxy-X04 labeling than the small ($\sim$10 μm) deposits which appeared in regions without plaques after capillary occlusions (Figure 1), so images for analysis of parenchymal plaques were not unmixed. Plaques were individually identified for tracking over time by referencing landmarks such as the blood vessels and other plaques. In control animals, the intensity of

methoxy-X04 labeling in the same plaque increased to 152% of baseline (median) after three days, while in plaques around a lesion, intensity increased to 112% of baseline (Figure 2(d)). In control animals, the area of a plaque increased to a median of 142% of baseline, while in lesioned animals, plaques stayed about the same size with a median of 97% of baseline (Figure 2(e)).
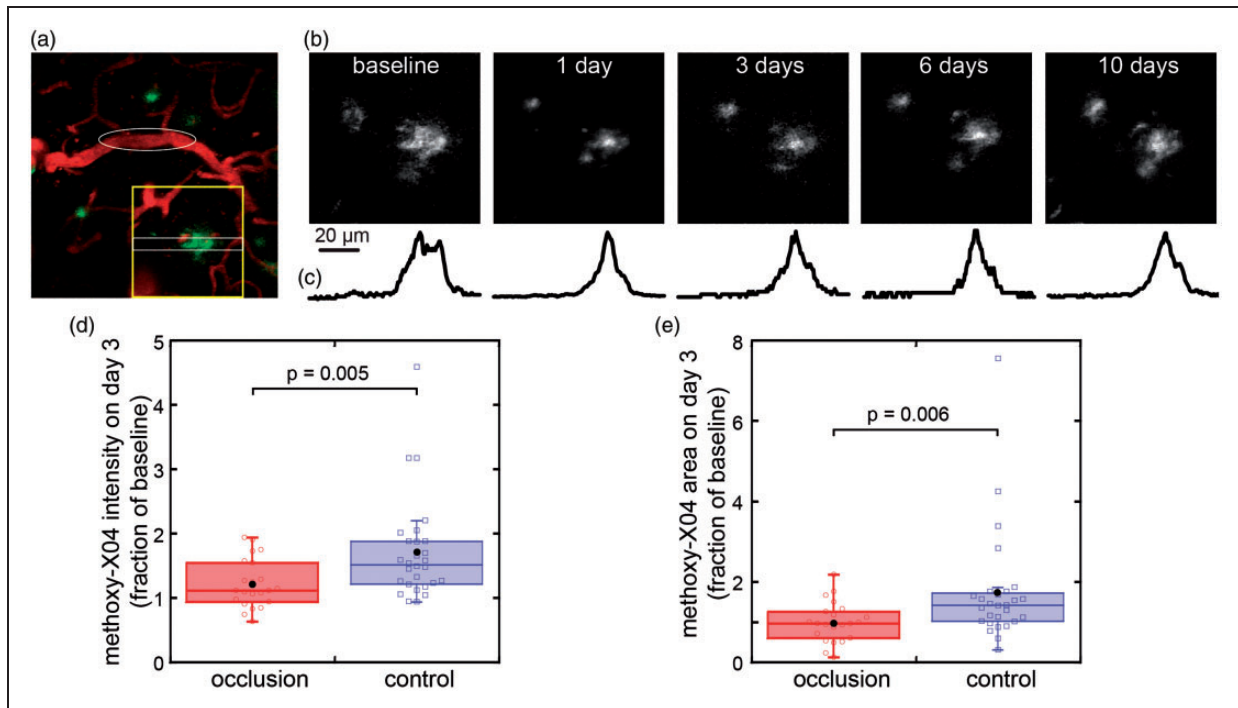
Figure 2. Pre-existing plaques change shape and size after occlusions of single subsurface vessels. (a) Vessels (red) and plaques (methoxy-X04, green) before occlusion. Target vessel for occlusion, a subsurface, pre-capillary arteriole, is indicated by white ellipse. (b) Methoxy-X04 labeling of plaques near the occlusion was imaged over time (region indicated by yellow box in (a)). Images are maximum intensity projections though 50 μm and are median filtered for display. (c) Intensity profile over time normalized by peak value averaged in the y-direction in region of white box in (a). (d) Mean intensity and (e) area of methoxy-X04 labeling in the same plaques within 200 μm of the lesion at three days after occlusions of single subsurface capillaries or pre-capillary arterioles normalized to baseline images (22 plaques in occlusion group (n = 3 lesions in three animals, two males and one female, 12 months); 28 plaques in control in separate animals with no lesions (one male and one female, 12 months old)). Boxplot shows median and quartiles, black dot shows mean. p values are calculated from Wilcoxon–Mann–Whitney rank-sum test.

Figure 1. Continued
unmixing yielded images of methoxy-X04 (blue in (b) and (f), white in (d) and (h)) in CAA and other deposits, as well as auto-fluorescence signals (green in (b) and (f), white in (c) and (g)). (i–p) Time-lapse imaging of methoxy-X04 deposits near a pre-capillary arteriole occluded by femtosecond laser ablation. Texas-red dextran was injected in the vasculature to visualize vessels (red, panels (i)–(l)). Unmixed methoxy-X04 channel (white, panels (m)–(p)) is displayed with same normalization across days. Punctate methoxy-X04 deposits in regions without pre-existing, large, parenchymal plaques observed after occlusions of single subsurface vessels in APP/PS1 animals. Arrows indicate deposits identified by automated segmentation. (q) Quantification of number of methoxy-X04 and (u) autofluorescent deposits in AD mice within 50 μm of the occluded vessel. (r and v) Similar vessels with no lesions were imaged within the same cortical windows in AD animals for control. (s) Area of each deposit of methoxy-X04 and (w) autofluorescence after lesion and (t and x) in control. AD with lesions: 27 lesions in eight animals, 11 to 15 months in age, six males and two females; AD with no lesions: 26 vessels in nine animals, five males and four females, 11 to 16 months in age. Significance tested within each graph by ANOVA with post hoc Tukey's test. Comparisons at same time points of AD with and without lesions were tested with Wilcoxon–Mann–Whitney rank-sum test. Black dots show means. AD: Alzheimer's disease.
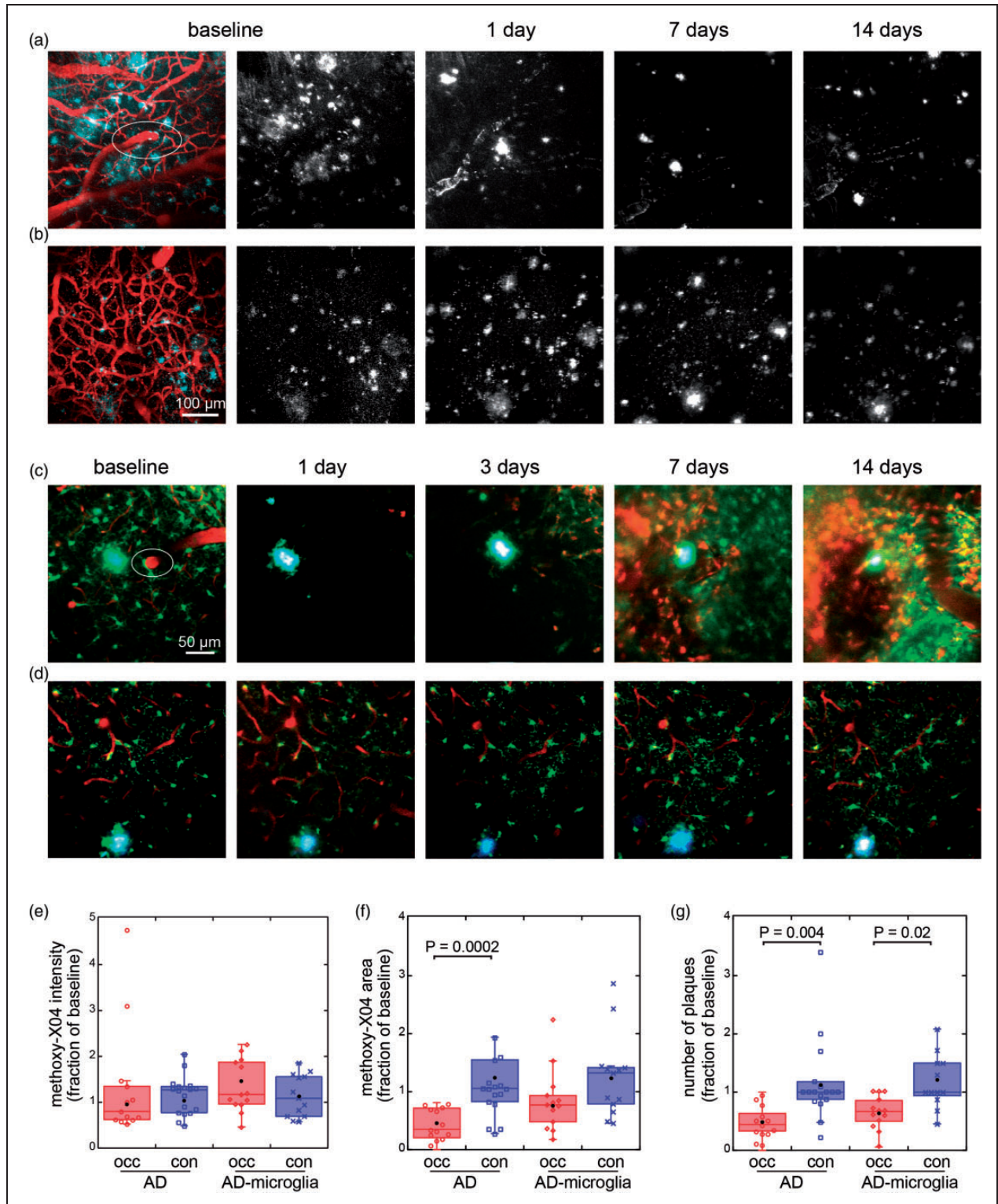
Figure 3. In vivo imaging of plaque and microglia dynamics after an ischemic lesion induced by rose bengal photothrombosis of a penetrating arteriole. (a) Plaques in an APP/PS1 animal are visualized with methoxy-X04 (cyan and white) and vessels by Texas-red dextran injection (red). White ellipse indicates targeted penetrating arteriole. (b) Control region imaged in animal with no lesions. Images in (a) and (b) are maximum projections displayed with median filtering. (c) Penetrating arteriole occlusion in an AD-microglia mouse. Microglia (Cx3cr1-GFP) are shown in green, blood vessels in red, and methoxy-X04 in cyan. (d) Contralateral side of the same mouse was imaged as control. The images in (c) and (d) are average projections of 20 μm. Contrast of each channel was adjusted for

We then imaged pre-existing plaques in a more severe model of focal stroke in which we occluded a penetrating arteriole (Figure 3).[26,28,34] This stroke model also led to the occlusion of some capillaries within a ~200 μm diameter region around the targeted vessel. Because both Aβ accumulation and vascular lesions affect microglia, we also used APP/PS1 mice that express GFP in microglia, here referred to as AD-microglia mice (Figure 3(c)). After the lesion, we observed several changes that followed the same trends in both types of mice. One day after the lesion, many of the larger, diffusely labeled plaques decreased in area, while the methoxy-X04 signal became brighter at the center of some plaques. In addition, other plaques appeared to decrease in intensity of labeling and some plaques disappeared. The condensation and "brightening" of larger plaques and the disappearance of smaller deposits was more pronounced about a week after the lesion. Alterations in appearance of the deposits were stabilized by two weeks after the lesion. These lesions were also accompanied by an accumulation of red autofluorescent deposits. The tissue rearranged after these injuries and some of the vasculature, which we used for landmarks, was altered, so for quantitative comparisons, projections were taken in approximately the same image volumes that were identified by the vasculature before and one day after the lesioning. At one day after lesioning in both strains of mice, the intensity of plaques was statistically unchanged but highly variable (Figure 3(e)). Both the area of methoxy-X04 labeling and the number of plaques in regions within ~1 mm of the lesion were reduced when compared to controls (Figure 3(f)), and the number of plaques at the lesion decreased to a median of 44% of baseline levels in APP/PS1 mice and to a median of 67% in AD-microglia mice (Figure 3(g)).

Penetrating arteriole occlusion causes both disappearance and appearance of plaques

In AD-microglia mice, the numbers of plaques were sufficiently sparse to enable us to individually track a subset of plaques over two weeks after a penetrating arteriole occlusion and in the hemisphere contralateral to the lesion (Figure 4 and Supplementary Figure 5). In individually identified plaques, the methoxy-X04 labeling intensities on average increased, but with high variation between plaques at one and three days after the lesion. Methoxy-X04 labeling intensity returned to baseline after two weeks (Figure 4(b)). The change in area of individual plaques was also variable (Figure 4(c)), and manual tracking of landmarks such as vessels confirmed that some plaques disappeared (Figure 4(d) and Supplementary Figure 5). We found that only about two-third of the plaques visible before lesioning were still visible at three or four days after the lesion using both in vivo imaging and anti-Aβ stained tissues (Figure 4(d) and (e) and Supplementary Figure 10). A subset (12%) of the plaques that were visible with methoxy-X04 at baseline disappeared temporarily and then reappeared over the course of two weeks. On the contralateral hemisphere, no plaques disappeared (Figure 4(e) and Supplementary Figure 5(b)). A small number of new plaques appeared on both sides, although the lesion side had a higher rate of appearance (23% of baseline plaques) than the contralateral control (12% of baseline plaques).

Aβ plaque disappearance correlates with appearance of non-fibrillar Aβ protein at lesion center after a penetrating arteriole occlusion

In sectioned tissue harvested one and four days after the penetrating arteriole occlusion, the lesion was easily visualized by abnormal axons and loss of cell bodies of YFP-expressing neurons. We defined the center of this region, around 300-400 μm below the cortical surface, as the lesion center to facilitate spatial comparisons. One day after lesion, anti-Aβ immunostaining showed increased intensity compared to the control region on the contralateral side which was distributed diffusely in an ellipsoidal volume at the lesion center that was largely gone at four days (Figure 5). Sections processed without primary antibody showed no intensity difference, suggesting the labeling increase reflects Aβ proteins (Supplementary Figure 7). Normalized average anti-Aβ intensity verified that anti-Aβ labeling transiently increased significantly one day after occlusion but returned close to control values by day 4 (Figure 5 (e) and (f)). On day 4, although the average anti-Aβ labeling intensity was reduced near the lesion center to

Figure 3. Continued
best view in the baseline images. The contrasts of images from the subsequent days are displayed so that the mean of manually chosen background regions appears the same across days. (e) Mean intensity and (f) area of methoxy-X04 labeling, and (g) number of plaques at one day after lesion (occ) and in control (con) in the image region with values all normalized to baseline in APP/PS1 (occlusion: 13 lesions in 13 animals, 8 males and 5 females, controls: 10 males and 7 females, 8–12 months old) and AD-microglia mice (13 lesions in 13 animals, 5 males and 8 females, 8–10 months old). (f) Outliers not shown on graph (AD, control: 5.9, 8.21). (g) Outliers not shown on graph (AD, control: 3.4, 4.6). Data were plotted so that each dot represents one animal. Black dots show means. p values calculated from Wilcoxon–Mann–Whitney rank-sum test. AD: Alzheimer's disease.
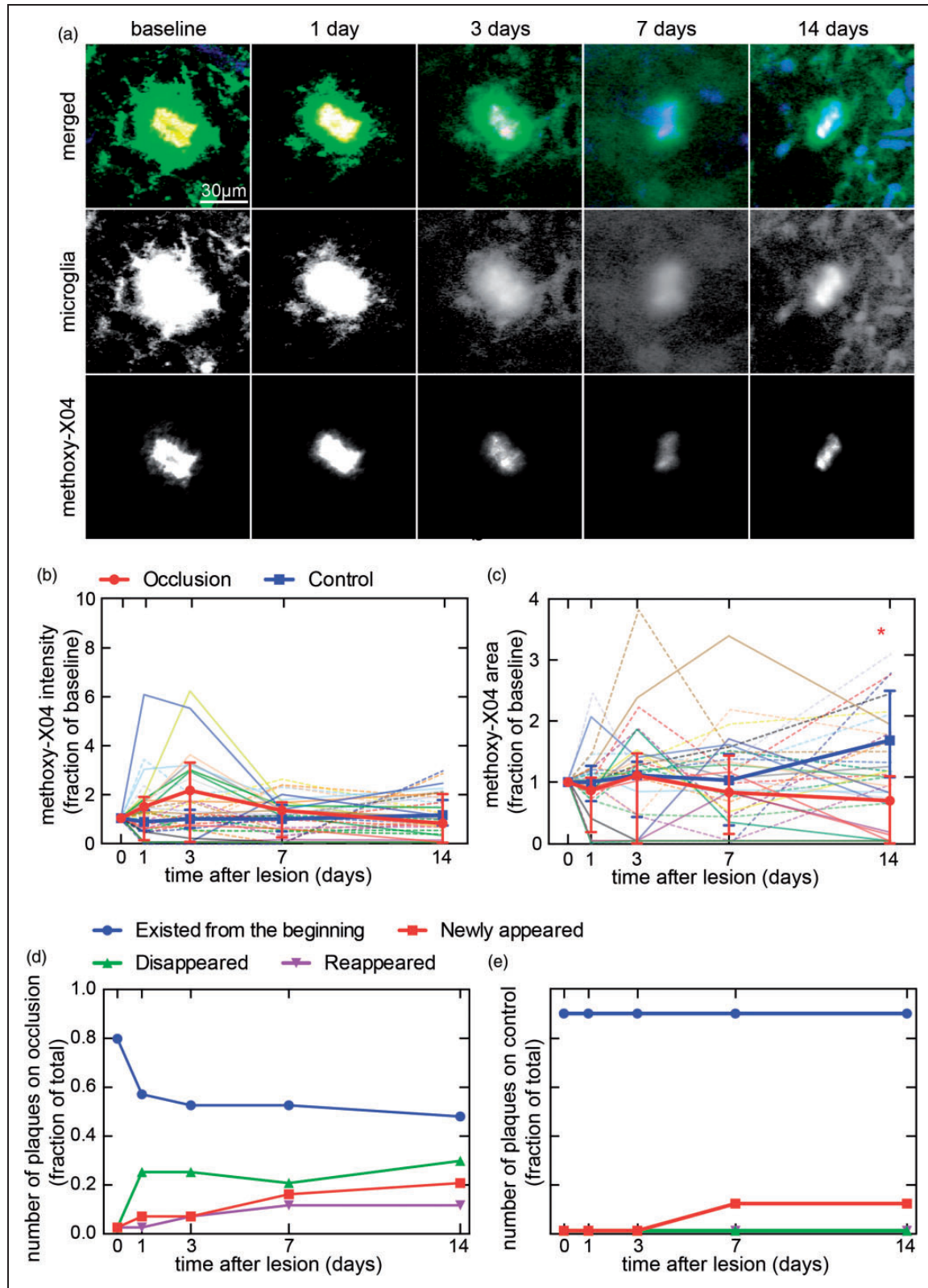
Figure 4. Two-photon microscopy images of plaques and microglia, and quantification of individually identified plaques after a penetrating arteriole occlusion. (a) An example plaque near penetrating arteriole occlusion. Microglia (Cx3cr1-GFP in green), plaques (methoxy-X04 in red), and blood vessels (Texas-red in blue) in AD-microglia mice after occlusion of a penetrating arteriole. Methoxy-X04 deposits overlapped spatially with GFP-labeled microglia, so show up as yellow in the merged images. Images were median

control levels, anti-Aβ labeling remained bright in isolated clumps that were not colabeled by methoxy-X04 (Figure 5(b) and (f)). Methoxy-X04, which labels fibrillar Aβ, appeared in a pattern distinct from the anti-Aβ antibody. There were almost no Aβ plaques labeled by methoxy-X04 within the lesion center, but methoxy-X04 plaques were present all around the lesion (Figure 5(a) and (b)). One day after the occlusion, the number of methoxy-X04-labeled plaques in regions with increased anti-Aβ labeling around the lesion center decreased to 20% relative to the neighboring regions, with the trend continuing on day 4 (Figure 5 (g) and (h)). However, changes in methoxy-X04 distribution were not evident in spatially average intensity of methoxy-X04 likely due to the sparse distribution of plaques (Supplementary Figure 8).

Cx3cr1-GFP microglia population changes coincide with alterations in plaques after penetrating arteriole occlusions

Microglia dynamics were visualized by the GFP in AD-microglia mice during in vivo imaging and in tissue sections. At baseline, plaque-associated microglia clustered densely around and within methoxy-X04-labeled deposits. Microglia not immediately adjacent to the plaques were ramified and scattered throughout the parenchyma. One day after occlusion, in vivo imaging in the top 150 μm of cortex showed that the GFP signal in parenchymal microglia became very faint in the immediate ~200 μm radius of the occluded vessel (Figure 3(c)), but the total number of microglia stayed about constant (Figure 6(a)). In plaque-associated microglia in this region, GFP labeling lingered with higher intensities than in parenchymal microglia (Figure 4(a), Supplementary Figure 5). Over the course of seven days, there was a large increase in microglia density relative to baseline in the region around the occluded vessel that remained on day 14 (Figures 3(c) and 6(a)). These microglia were not ramified and had larger cell bodies and fewer, shorter processes than the microglia at baseline or in control. In some cases, microglia changes were

accompanied with a shape change of the plaque (Figure 4(a)) or disappearance (Supplementary Figure 5(a)). There were no notable differences in area covered by microglia around plaques that stayed visible for at least three days or disappeared (Supplementary Figure 6). In control regions, contralateral from the lesions, microglia did not change in number or shape either near or far from plaques (Figures 3(d) and 6(c)). In sectioned tissue, we were able to observe microglia beyond the maximum two-photon imaging depth. Overall, microglia dynamics ex vivo followed trends similar to in vivo, but the increase in number was observed earlier, deeper in the tissue (Figure 6(b)). One day after the lesion, the number of microglia assessed by GFP visualization in sections doubled relative to the control at the lesion, with the greatest density centered around 300–400 μm below the surface, coinciding with the location of the diffuse anti-Aβ increase (Figure 6(c) to (e)). Closer to the cortical surface, the rate of increase in microglia number was slower than at the lesion center. Labeling with antibodies against IBA-1 showed similar patterns to GFP and there was no significant difference in ratios of GFP and IBA-1 between lesioned and control regions at any time point (Supplementary Figure 11).

Non-fibrillar Aβ coalesces at microglia after four days in penetrating arteriole lesion

Four days after the lesion, the number of microglia quantified in tissue sections increased to 2.5 times the number on the contralateral side (Figure 6(b)) and tended to be spread over a larger area than at day 1 (Figure 6(c) and (d)). Microglia remained rounded compared to control. Three days earlier, at the lesion center where methoxy-X04 plaques had disappeared and diffuse anti-Aβ increased, microglia with shortened processes were observed near the new, anti-Aβ positive, methoxy-X04 negative, deposits (Figure 5(i) to (iv)). In comparison, at all time points, the regions away from the lesion contained parenchymal microglia with small cell bodies and long processes that were distinct from the morphologies of both the parenchymal microglia at

Figure 4. Continued

filtered with radius of one pixel and are summed projections of the log of intensities. (b) Intensity and (c) area of methoxy-X04 in individually identified plaques that were tracked over 14 days after a penetrating arteriole occlusion in AD-microglia mice (three lesions in three animals, two males and one female, 8–10 months old). Individual plaques from occlusion sites are represented by dim solid lines and plaques from control sites on the contralateral hemisphere of the same animals are plotted with dim dotted lines. Bold lines show medians with error bars representing interquartile ranges. Kruskal Wallis test shows no significant differences across the 14-day period in intensity, but significant differences in area (p = 0.0024), which was followed by multiple comparison analyses with Dunn's correction (*occlusion day 1 vs. occlusion day 14: p = 0.0028, occlusion day 14 vs. control day 14: p = 0.0005). In (b) and (c) plaques that disappeared were shown in the graph as having an intensity and area of zero. (d) Number of individually tracked plaques near the occlusion and (e) in control regions. Numbers are normalized by the cumulative number of plaques present during the two weeks.
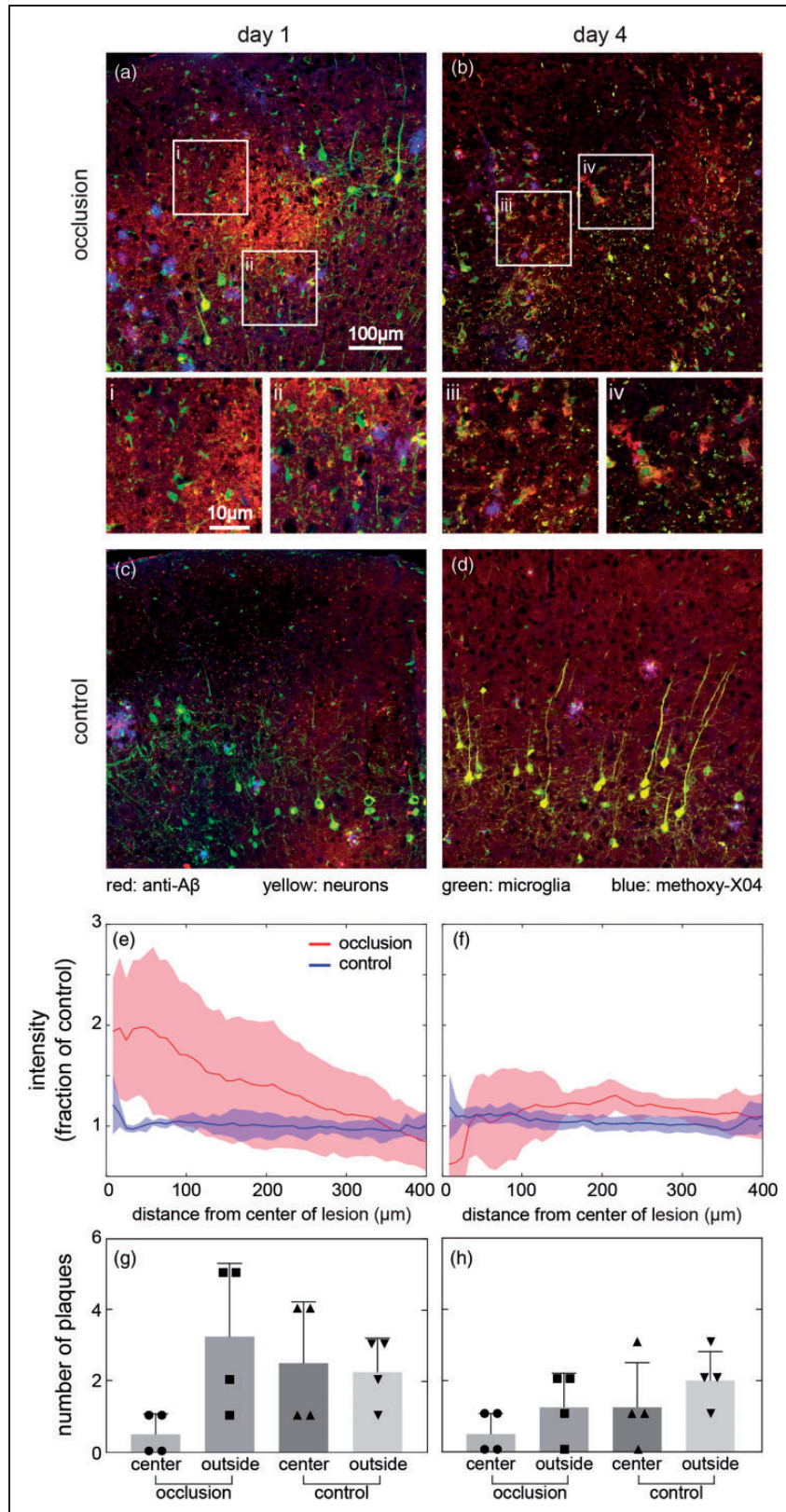
Figure 5. Immunohistology and quantification of Aβ protein one (left) and four (right) days after a penetrating arteriole occlusion. (a–d) Aβ immunostaining was performed on sections from AD-microglia mice one day (a) and four days (b) after occlusion. Control images were taken in the contralateral hemisphere (c and d). Aβ protein was visualized by anti-Aβ antibody (red), microglia by

lesions and plaque-associate microglia (Figure 6(c) to (e) and Supplementary Figure 9).

Closed-skull rose bengal stroke model showed increased labeling intensity for Aβ deposits at lesion margins

We also evaluated the effects of an even more severe model of stroke on Aβ deposits using photothrombosis in a ~1 mm area irradiated through the skull. This model of stroke leads to the occlusion of a large fraction of surface and sub-surface blood vessels in the irradiated region. After a 10-day survival, tissue was harvested and Aβ deposits were visualized using a pan-Aβ antibody. We found infarctions at the cortical surfaces of ~1-mm diameter that extended in depth through most of the cortex (Figure 7(a) and (c)). We analyzed Aβ deposits within 500 μm of the edge of the infarct and found that these deposits had increased intensity of labeling when compared to plaques found on the contralateral side with no lesion (Figure 7(e)). Both the area per plaque and the number of plaques showed a trend toward increasing around the infarct as compared to the contralateral
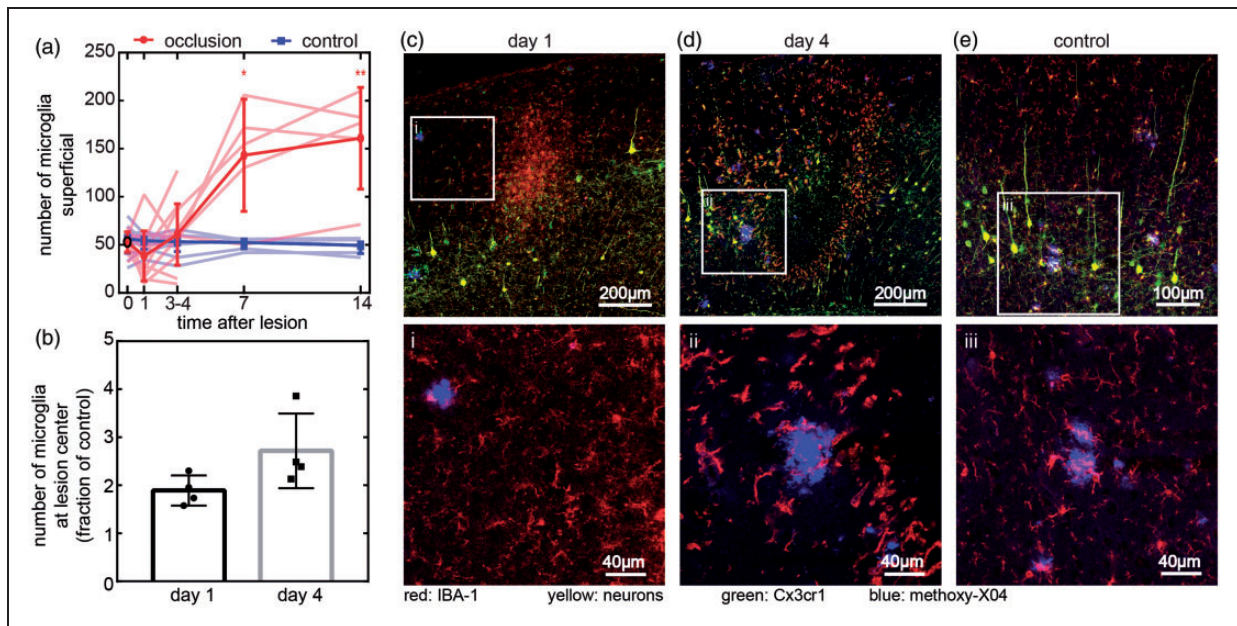
Figure 6. Microglia after a penetrating arteriole occlusion. (a) Quantification of microglia number from in vivo images at lesions in a $350 \times 350 \times 20\,\mu m$ volume near the cortical surface and in control sites on the contralateral hemisphere. Bold line shows mean and standard deviation. A subset of animals was harvested at four days and used for immunohistology, but data are shown pooled for all animals measured at each time point (n = 5 animals imaged for 14 days, three males and two females, 8–12 months old; n = 7 animals imaged for four days, four males and three females, 8–12 months old). Dim lines represent individual animals. Paired t-tests were used to compare experiment and control groups on the same day (*p = 0.03, **p = 0.01). (b) Microglia counted in a $500 \times 500\,\mu m$ square at lesion center in 20-μm tissue sections one and four days after lesion normalized to contralateral side (mean and standard deviation). Each dot represents one animal (n = 8 animals, day 1: one male and three females; day 4: two males and two females, 8–12 months old). (c–e) Representative images of sections one (c) and four days (d) after lesion. Microglia were visualized by both anti-IBA-1 antibody (red) and Cx3cr1-GFP (green), neurons express YFP (yellow), and plaques were stained by methoxy-X04 (blue). (e) Representative control image was taken from the contralateral hemisphere four days after lesioning. Images of contralateral hemisphere from one day after lesion shown in Supplementary Figure 9. White square regions show representative high magnification images (i–iii) from (c–e) with just methoxy-X04 and anti-IBA-1 shown for clarity.

Figure 5. Continued

Cx3cr1-GFP (green), neurons by YFP (yellow), and plaques by methoxy-X04 (blue). White square regions show representative high-magnification images (i–iv) from (a) and (b). Average anti-Aβ labeling intensity as a function of distance from the center of the lesion one day (e) and four days (f) after lesion. Solid line represents average anti-Aβ intensity and shaded area represents standard deviation. (g and h) Number of plaques inside and outside of the region of elevated anti-Aβ labeling near lesion center one day (g) and four days (h) after occlusion. Same-sized regions were evaluated on the contralateral side as control. Bar represents standard deviation and each dot represents one animal. A Kruskal–Wallis test showed no significant differences (day 1: one male and three females; day 4: two males and two females, 8–12 months old).
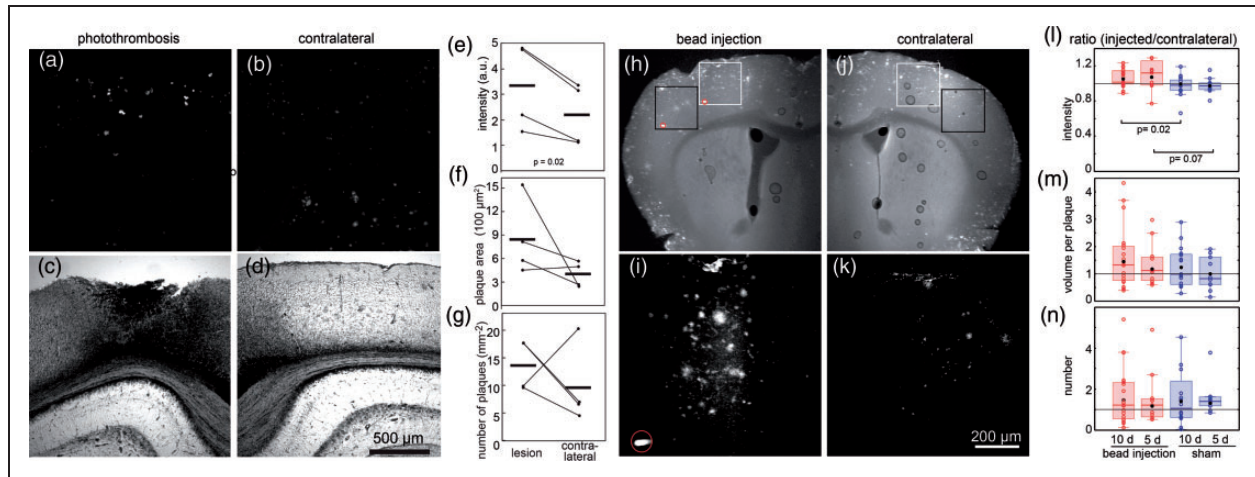
Figure 7. Anti-Aβ antibody labeling of lesions from 10-day survival after closed skull photothrombosis and embolic stroke. Aβ deposits in cortical sections were labeled with antibodies against anti-Aβ and detected with wide-field fluorescence (n = 4, ages 26–28 months, three females and one male). (a) Fluorescent image of anti-Aβ labeling on lesion side shows labeled plaques. (b) Contralateral cortex in same section used as control. (c and d) White light images shows disrupted tissue at lesion and intact tissue on contralateral control. (e–g) Comparison of anti-Aβ antibody labeling in tissue sections around lesion and on contralateral side in equivalent brain region. Bars show mean values. Wilcoxon rank sign test for paired values was used for p values. Unlisted p values were greater than 0.1. (h and i) Low-magnification multiphoton fluorescence images from bead injection (h) and contralateral side (i) of an animal that was sacrificed five days after bead injection in the embolic stroke model. Such images were used to find areas (boxes) near microbeads (red circles) and mirroring regions on the contralateral side. (j and k) Projection of 200-μm deep multiphoton image stacks (after background removal) labeled with anti-Aβ antibody. The images in (j) and (k) come from the white boxes in (h) and (i), respectively. (l–n) Quantification of labeling with anti-Aβ at 5 and 10 days after embolic stroke. Ratios between lesion and contralateral side for labeling intensity (l), volume per plaque (m), and number of plaques (n). Each point represents the mean value from an imaged region normalized by values from the corresponding region on the contralateral side. Black dot is mean, box shows median and quartiles. Outliers not shown: intensity (10 day bead, 2.1; 5 day bead, 2.5), number (10 sham, 13.5). Kruskal–Wallis rank-sum tests followed by Wilcoxon–Mann–Whitney rank-sum tests were used to evaluate significance. Unlisted p values were greater than 0.1. Animals survived five days (five mice with microbeads (three males and two females), two sham mice (one male and one female), 10–26 months old) or 10 days (seven mice with microbeads (four females and three males), four sham mice (one female and three males), 10–22 months old).

side, although these trends did not reach significance (Figure 7(f) and (g)).

Embolic stroke models also caused an increase in the intensity of labeling of Aβ deposits

Finally, we used another model of small-scale stroke in which vessels were occluded by injection of fluorescent microbeads into the internal carotid artery.[24] Beads with 25-μm diameter lodged in small arterioles or capillaries in the territory of the middle cerebral artery on the same side of the brain as the carotid artery injection. For the sham procedure, animals were injected with sterile saline. No obvious behavioral signs of stroke were seen in any of the animals, and we did not observe infarcts in any animal. Animals survived 5 days or 10 days before perfusion and histological analysis of Aβ deposits using anti-Aβ antibodies. The number of plaques was highly variable across animals, so we normalized measures of plaque properties from the side ipsilateral to the injection to the measurements taken in the equivalent region on the contralateral side of the same brain section

(Figure 7(h) to (k)). This normalization controls for differences between animals and enables a comparison between microbead-injected and sham animals. After five-day survival, the normalized intensity of the labeling of plaques was increased by more than 10% in lesioned animals compared to sham, with this increase still present but diminishing in the 10-day survival animals (Figure 7 (l)). While there was a slight trend for an increase in normalized plaque volume after microbead injection with 5- and 10-day survivals when compared to the sham experiments, the variability in the data was high and the trend did not reach significance (Figure 7(m)). The normalized number of plaques did not appear different between lesioned and sham animals (Figure 7(n)).

Discussion

Morphological changes in pre-existing amyloid plaques after ischemic lesions

Histological studies have suggested that "diffuse" plaques might transition to "dense" or "dense core"

plaques under conditions such as injury.[11,35] Using time lapse imaging of the small lesions from occlusions of single or a few capillaries or arterioles, we showed that pre-existing plaques that were diffusely labeled with methoxy-X04 can appear to condense, with labeling concentrating toward the center of the plaque, although on average the total intensity of the labeling did not increase (Figures 2 and 3). In the single subsurface capillary occlusion model, this effect appeared to relax somewhat over two weeks (Figure 2). In more severe injuries, it was not clear whether this condensation was reversible over a similar timeframe (Figure 4(a)). It is not known whether these plaque changes occur in humans, but the observation of both diffuse and dense plaque morphologies in humans suggests that these findings may be clinically relevant.[35,36]

Disappearance and appearance of Aβ plaques after microstrokes

Several previous imaging studies showed that $A\beta$ deposits can disappear after treatments such as anti-$A\beta$ antibodies.[12,37–39] Time-lapse imaging with methoxy-X04 revealed a natural cause of disappearance by showing some pre-existing plaques disappeared near the occlusions of penetrating arterioles, although a fraction of these plaques also reappeared over two weeks (Figure 4). Methoxy-X04 labeling of fibrillary $A\beta$ lasts up to 90 days, thus plaque disappearance was unlikely to be due to turnover of methoxy-X04.[40] The occlusion of a penetrating arteriole induces a more severe drop in blood flow than the occlusion of a subsurface capillary,[25,26] after which we did not observe disappearance of plaques. This suggests that a minimum level of blood flow change, injury, or inflammation is required for plaques to disappear. In both the lesioned and control hemisphere of the AD-microglia mice, there was a high rate of newly formed plaques compared to previous studies,[41–44] which might be explained by both local and systemic effects of the lesion. The net result in the immediate area around the penetrating arteriole occlusion is a decrease in the number of plaques at two weeks, despite an increase in the rate of appearance of new plaques. Two alternate kinds of ischemic injuries, a larger infarct and embolic stroke (Figure 7), increased intensity and number of plaques reminiscent of the higher rate of plaque formation after penetrating arteriole occlusion. The dynamics of $A\beta$ deposits likely sensitively depend on parameters of the injury. In the penetrating arteriole occlusion model, the decrease in $A\beta$ deposits was primarily observed in the center of lesion (i.e., "core") where the tissue was disrupted but intact (Figure 5). However, in the intact-skull model where the infarct was larger, tissue at the "core" of the lesion disintegrated so analysis is only in the margins where $A\beta$ labeling increased. In the embolic stroke model, the injection of beads resulted in minimal tissue damage with no infarct, potentially suggesting that the tissue damage was not severe enough to cause plaque disappearance.

Microstrokes drive a transition between plaques and non-fibrillar Aβ

The disappearance of methoxy-X04 plaques one day after a penetrating arteriole occlusion coincides with the appearance of delocalized, diffuse $A\beta$, revealed by antibody labeling (Figure 5). This new deposit did not colabel with methoxy-X04 suggesting that lesions cause production of non-fibrillar forms of $A\beta$ or, alternatively, conversion of pre-existing $A\beta$ from plaques to a non-fibrillar form. The non-fibrillar and soluble forms of $A\beta$ aggregates have been associated with neurotoxicity,[45,46] which implies that occlusions in small vessels or microstrokes could worsen AD progression even if the plaque number is reduced. The spatial and temporal correlation between $A\beta$ changes and microglia dynamics suggests a role for inflammatory cells in this process that needs future investigation. The new anti-$A\beta$-labeled aggregates found at the lesion center on day 4 had nearby microglia, supporting a role for microglia in transitions of $A\beta$ deposit morphologies after the lesion (Figure 5(iii) to (iv)). The small, cell-sized methoxy-X04 deposits that appeared after the occlusion of capillaries (Figure 1 and Supplementary Figure 4) suggests the involvement of phagocytosis of $A\beta$ by microglia or other cells such as astrocytes.[12,39] The microglia near the $A\beta$ plaques that survived lesioning had more robust GFP signal than parenchymal microglia (Figure 4(a)), consistent with the idea that the plaque-associated microglia are functionally different from the other microglia.[47] Vascular injuries are triggers for inflammatory cascades that can add to inflammation that is already present in the AD brain. Many other cells such as monocytes and astrocytes play a role in phagocytosis of plaques and these cells also activate during ischemia and stroke, but were not investigated here.[48–54] We also caution that we cannot clearly distinguish between resident and invading cells, so that the Cx3cr1-GFP cells characterized here could originate from circulating cells. Although we observed similar plaque dynamics after injury between AD and AD-microglia mice, it is worth noting that the Cx3cr1-GFP mouse model has one copy of Cx3cr1 chemokine receptor replaced by GFP, which could have a potential impact in plaque recognition and clearance.[51,55]

Imaging in Aβ deposition and lesion studies

This study revealed several experimental aspects that can complicate multiphoton microscopy imaging studies of Aβ in mouse models. First, our finding that the vascular injury can change plaques from diffuse to dense and back again suggests that many kinds of injury or inflammation might have this effect. This suggests that other studies using cranial windows, which can cause inflammation in brain tissue, may need to contend with the effects described here.[56] In this study, we used open cranial windows, which had been implanted for at least three weeks and in some cases several months, to minimize the effects of the cranial window. We cannot rule out the effects of the window and imaging, although we saw similar results without cranial windows. The other cautionary result from this work is that autofluorescence in imaging studies can be quite bright, cell-shaped and confounding because it correlates with the experimental treatment. Some autofluorescence, including the red autofluorescence (e.g., in Figures 1 and 3(c)), is likely related to cell stress and injury and therefore is associated with the strokes induced here.[57] In this work, we found that the spectral properties of methoxy-X04, the standard for multiphoton microscopy of Aβ plaques, are similar to autofluorescent signals produced around vascular lesions. We found that it is possible to unmix these signals and that methoxy-X04 and autofluorescence signals appear in separate volumes. It is unclear how previous in vivo imaging studies of Aβ changes after stroke handled this complication.

There are some limitations in our methods that may bias the types of plaques analyzed. Methoxy-X04 was injected before each imaging session, and because the labeling from previous imaging sessions is still present, stable plaques accumulate more labeling with each imaging session. Our finding that in control animals, plaques increased in size and intensity over time is consistent with this mechanism and the literature.[41,42] The regions measured could also have some selection bias, because regions were chosen where it was possible to identify what appeared to be the same vessels at both time points. In an attempt to reduce bias, the thresholding algorithm was based on quantitative measures as much as possible (the user still had to choose background regions manually). It was not practical to blind the analysis because the difference between lesioned and unlesioned images was too clear. In vivo imaging analysis was limited to the upper cortical region after penetrating arteriole occlusions. The lesion has a depth-dependent structure that may be related to the cell types or vascular structures found in different layers in cortex.[34] The increase in anti-Aβ labeling as well as the accumulation of microglia was centered around layer 4 or 5. This resulted in some differences between measurements with in vivo imaging, which only went ~200 μm deep, and postmortem, sectioned tissue.

Conclusions

The emerging picture is that vascular injury certainly alters Aβ accumulation, but it is much more complex that a simple increase or decrease. Even around a single lesion, the heterogeneity of plaque dynamics suggests that Aβ is highly sensitive to local physiology such as regional variations in blood flow[54,58] and tissue structure. Here, we found complex dynamics in Aβ deposits after multiple models of mild or small strokes that could reflect a redistribution of Aβ within the tissue in response to injury and inflammation as well as changes in total amount. We did not investigate factors such as sex or environment that have known modifiers of both AD and vascular health,[59] but these could be important for our understanding of the disease in clinical populations. This work demonstrates that vascular pathology and prior injury can influence AD and because microvascular pathology and cardiovascular risk factors are common in AD, the mutability of Aβ deposits must be considered when using plaques as a marker for AD progression.

Declaration of conflicting interests

The author(s) declared no potential conflicts of interest with respect to the research, authorship, and/or publication of this article.

Authors' contributions

YZ performed experiments and analysis on microglial mice and contributed to writing. EDB, YL, and CM conducted experiments on embolic stroke model and analysis and contributed to writing the manuscript. CBS designed experiments and contributed to analysis and writing. NN supervised,

performed remaining experiments and analysis, and contributed to writing.

ORCID iD

Nozomi Nishimura (iD) https://orcid.org/0000-0003-4342-9416

Supplementary material

Supplemental material for this article is available online.

References

1. Snowdon DA. Healthy aging and dementia: findings from the Nun Study. *Ann Intern Med* 2003; 139: 450–454.
2. Iadecola C. Neurovascular regulation in the normal brain and in Alzheimer's disease. *Nat Rev Neurosci* 2004; 5: 347–360.
3. de la Torre JC. Is Alzheimer's disease a neurodegenerative or a vascular disorder? Data, dogma, and dialectics. *Lancet Neurol* 2004; 3: 184–190.
4. Vinters HV, Ellis WG, Zarow C, et al. Neuropathologic substrates of ischemic vascular dementia. *J Neuropathol Exp Neurol* 2000; 59: 931–945.
5. Castellani RJ, Smith MA, Perry G, et al. Cerebral amyloid angiopathy: major contributor or decorative response to Alzheimer's disease pathogenesis. *Neurobiol Aging* 2004; 25: 599–602; discussion 603–594.
6. Jellinger KA. Alzheimer 100–highlights in the history of Alzheimer research. *J Neural Transm* 2006; 113: 1603–1623.
7. Mawuenyega KG, Sigurdson W, Ovod V, et al. Decreased clearance of CNS beta-amyloid in Alzheimer's disease. *Science* 2010; 330: 1774.
8. Tanzi RE, Moir RD and Wagner SL. Clearance of Alzheimer's Abeta peptide: the many roads to perdition. *Neuron* 2004; 43: 605–608.
9. Bateman RJ, Munsell LY, Morris JC, et al. Human amyloid-beta synthesis and clearance rates as measured in cerebrospinal fluid in vivo. *Nat Med* 2006; 12: 856–861.
10. Iliff JJ, Wang M, Liao Y, et al. A paravascular pathway facilitates CSF flow through the brain parenchyma and the clearance of interstitial solutes, including amyloid beta. *Sci Translat Med* 2012; 4: 147ra111.
11. van Groen T, Puurunen K, Maki HM, et al. Transformation of diffuse beta-amyloid precursor protein and beta-amyloid deposits to plaques in the thalamus after transient occlusion of the middle cerebral artery in rats. *Stroke* 2005; 36: 1551–1556.
12. Popa-Wagner A, Schroder E, Walker LC, et al. beta-Amyloid precursor protein and ss-amyloid peptide immunoreactivity in the rat brain after middle cerebral artery occlusion: effect of age. *Stroke* 1998; 29: 2196–2202.
13. Garcia-Alloza M, Gregory J, Kuchibhotla KV, et al. Cerebrovascular lesions induce transient beta-amyloid deposition. *Brain* 2011; 134: 3697–3707.
14. Okamoto Y, Yamamoto T, Kalaria RN, et al. Cerebral hypoperfusion accelerates cerebral amyloid angiopathy and promotes cortical microinfarcts. *Acta Neuropathol* 2012; 123: 381–394.
15. Thal DR, Capetillo-Zarate E, Larionov S, et al. Capillary cerebral amyloid angiopathy is associated with vessel occlusion and cerebral blood flow disturbances. *Neurobiol Aging* 2009; 30: 1936–1948.
16. Green KN, Boyle JP and Peers C. Hypoxia potentiates exocytosis and Ca2+ channels in PC12 cells via increased amyloid beta peptide formation and reactive oxygen species generation. *J Physiol* 2002; 541: 1013–1023.
17. Carnevale D, Mascio G, D'Andrea I, et al. Hypertension induces brain beta-amyloid accumulation, cognitive impairment, and memory deterioration through activation of receptor for advanced glycation end products in brain vasculature. *Hypertension* 2012; 60: 188–197.
18. Koistinaho M and Koistinaho J. Interactions between Alzheimer's disease and cerebral ischemia–focus on inflammation. *Brain Res Brain Res Rev* 2005; 48: 240–250.
19. Mildner A, Schlevogt B, Kierdorf K, et al. Distinct and non-redundant roles of microglia and myeloid subsets in mouse models of Alzheimer's disease. *J Neurosci* 2011; 31: 11159–11171.
20. Yamada M, Ihara M, Okamoto Y, et al. The influence of chronic cerebral hypoperfusion on cognitive function and amyloid beta metabolism in APP overexpressing mice. *PLoS One* 2011; 6: e16567.
21. Lee JS, Im DS, An YS, et al. Chronic cerebral hypoperfusion in a mouse model of Alzheimer's disease: an additional contributing factor of cognitive impairment. *Neurosci Lett* 2011; 489: 84–88.
22. Koike MA, Garcia FG, Kitazawa M, et al. Long term changes in phospho-APP and tau aggregation in the 3xTg-AD mice following cerebral ischemia. *Neurosci Lett* 2011; 495: 55–59.
23. Cherry JD, Olschowka JA and O'Banion MK. Arginase 1+ microglia reduce Abeta plaque deposition during IL-1beta-dependent neuroinflammation. *J Neuroinflammation* 2015; 12: 203.
24. Nishimura N, Schaffer CB, Friedman B, et al. Targeted insult to subsurface cortical blood vessels using ultrashort laser pulses: three models of stroke. *Nat Methods* 2006; 3: 99–108.
25. Nishimura N, Schaffer CB, Friedman B, et al. Penetrating arterioles are a bottleneck in the perfusion of neocortex. *Proc Natl Acad Sci U S A* 2007; 104: 365–370.
26. Nishimura N, Rosidi NL, Iadecola C, et al. Limitations of collateral flow after occlusion of a single cortical penetrating arteriole. *J Cereb Blood Flow Metab* 2010; 30: 1914–1927.
27. Shih AY, Blinder P, Tsai PS, et al. The smallest stroke: occlusion of one penetrating vessel leads to infarction and a cognitive deficit. *Nat Neurosci* 2013; 16: 55–63.
28. Watson BD, Dietrich WD, Busto R, et al. Induction of reproducible brain infarction by photochemically initiated thrombosis. *Ann Neurol* 1985; 17: 497–504.
29. Silasi G, She J, Boyd JD, et al. A mouse model of small-vessel disease that produces brain-wide-identified micro-occlusions and regionally selective neuronal injury. *J Cereb Blood Flow Metab* 2015; 35: 734–738.

30. Jankowsky JL, Fadale DJ, Anderson J, et al. Mutant presenilins specifically elevate the levels of the 42 residue beta-amyloid peptide in vivo: evidence for augmentation of a 42-specific gamma secretase. *Hum Mol Genet* 2004; 13: 159–170.

31. Jung S, Aliberti J, Graemmel P, et al. Analysis of fractalkine receptor CX(3)CR1 function by targeted deletion and green fluorescent protein reporter gene insertion. *Mol Cell Biol* 2000; 20: 4106–4114.

32. Klunk WE, Bacskai BJ, Mathis CA, et al. Imaging Abeta plaques in living transgenic mice with multiphoton microscopy and methoxy-X04, a systemically administered Congo red derivative. *J Neuropathol Exp Neurol* 2002; 61: 797–805.

33. Pologruto TA, Sabatini BL and Svoboda K. ScanImage: flexible software for operating laser scanning microscopes. *Biomed Eng Online* 2003; 2: 13.

34. Taylor ZJ, Hui ES, Watson AN, et al. Microvascular basis for growth of small infarcts following occlusion of single penetrating arterioles in mouse cortex. *J Cereb Blood Flow Metab* 2016; 36: 1357–1373.

35. Kumar-Singh S, Cras P, Wang R, et al. Dense-core senile plaques in the Flemish variant of Alzheimer's disease are vasocentric. *Am J Pathol* 2002; 161: 507–520.

36. Akiyama H, Mori H, Saido T, et al. Occurrence of the diffuse amyloid beta-protein (Abeta) deposits with numerous Abeta-containing glial cells in the cerebral cortex of patients with Alzheimer's disease. *Glia* 1999; 25: 324–331.

37. Bacskai BJ, Kajdasz ST, Christie RH, et al. Imaging of amyloid-beta deposits in brains of living mice permits direct observation of clearance of plaques with immunotherapy. *Nat Med* 2001; 7: 369–372.

38. Garcia-Alloza M, Borrelli LA, Rozkalne A, et al. Curcumin labels amyloid pathology in vivo, disrupts existing plaques, and partially restores distorted neurites in an Alzheimer mouse model. *J Neurochem* 2007; 102: 1095–1104.

39. Wang A, Das P, Switzer RC III, et al. Robust amyloid clearance in a mouse model of Alzheimer's disease provides novel insights into the mechanism of amyloid-beta immunotherapy. *J Neurosci* 2011; 31: 4124–4136.

40. Condello C, Schain A and Grutzendler J. Multicolor time-stamp reveals the dynamics and toxicity of amyloid deposition. *Sci Rep* 2011; 1: 19.

41. Christie RH, Bacskai BJ, Zipfel WR, et al. Growth arrest of individual senile plaques in a model of Alzheimer's disease observed by in vivo multiphoton microscopy. *J Neurosci* 2001; 21: 858–864.

42. Burgold S, Filser S, Dorostkar MM, et al. In vivo imaging reveals sigmoidal growth kinetic of beta-amyloid plaques. *Acta Neuropathol Commun* 2014; 2: 30.

43. Burgold S, Bittner T, Dorostkar MM, et al. In vivo multiphoton imaging reveals gradual growth of newborn amyloid plaques over weeks. *Acta Neuropathol* 2011; 121: 327–335.

44. Meyer-Luehmann M, Spires-Jones TL, Prada C, et al. Rapid appearance and local toxicity of amyloid-beta plaques in a mouse model of Alzheimer's disease. *Nature* 2008; 451: 720–724.

45. Lue LF, Kuo YM, Roher AE, et al. Soluble amyloid beta peptide concentration as a predictor of synaptic change in Alzheimer's disease. *Am J Pathol* 1999; 155: 853–862.

46. Busche MA, Chen X, Henning HA, et al. Critical role of soluble amyloid-beta for early hippocampal hyperactivity in a mouse model of Alzheimer's disease. *Proc Natl Acad Sci U S A* 2012; 109: 8740–8745.

47. Keren-Shaul H, Spinrad A, Weiner A, et al. A unique microglia type associated with restricting development of Alzheimer's disease. *Cell* 2017; 169: 1276–1290.e1217.

48. Bolmont T, Haiss F, Eicke D, et al. Dynamics of the microglial/amyloid interaction indicate a role in plaque maintenance. *J Neurosci* 2008; 28: 4283–4292.

49. Wyss-Coray T, Loike JD, Brionne TC, et al. Adult mouse astrocytes degrade amyloid-beta in vitro and in situ. *Nat Med* 2003; 9: 453–457.

50. Hickman SE, Allison EK and El Khoury J. Microglial dysfunction and defective beta-amyloid clearance pathways in aging Alzheimer's disease mice. *J Neurosci* 2008; 28: 8354–8360.

51. Lee S, Varvel NH, Konerth ME, et al. CX3CR1 deficiency alters microglial activation and reduces beta-amyloid deposition in two Alzheimer's disease mouse models. *Am J Pathol* 2010; 177: 2549–2562.

52. Nihashi T, Inao S, Kajita Y, et al. Expression and distribution of beta amyloid precursor protein and beta amyloid peptide in reactive astrocytes after transient middle cerebral artery occlusion. *Acta Neurochir (Wien)* 2001; 143: 287–295.

53. D'Andrea MR, Cole GM and Ard MD. The microglial phagocytic role with specific plaque types in the Alzheimer disease brain. *Neurobiol Aging* 2004; 25: 675–683.

54. Masuda T, Croom D, Hida H, et al. Capillary blood flow around microglial somata determines dynamics of microglial processes in ischemic conditions. *Glia* 2011; 59: 1744–1753.

55. Liu Z, Condello C, Schain A, et al. CX3CR1 in microglia regulates brain amyloid deposition through selective protofibrillar amyloid-beta phagocytosis. *J Neurosci* 2010; 30: 17091–17101.

56. Xu H, Pan F, Yang G, et al. Choice of cranial window type for in vivo imaging affects dendritic spine turnover in the cortex. *Nat Neurosci* 2007; 10: 549–551.

57. De Los Angeles A, Ferrari F, Fujiwara Y, et al. Failure to replicate the STAP cell phenomenon. *Nature* 2015; 525: E6–E9.

58. Cruz Hernandez JC, Bracko O, Kersbergen CJ, et al. Neutrophil adhesion in brain capillaries reduces cortical blood flow and impairs memory function in Alzheimer's disease mouse models. *Nat Neurosci* 2019; 22: 413.

59. Cacciottolo M, Christensen A, Moser A, et al. The APOE4 allele shows opposite sex bias in microbleeds and Alzheimer's disease of humans and mice. *Neurobiol Aging* 2016; 37: 47–57.